JOURNAL OF MATERIALS SCIENCE 29 (1994) 4953–4961

Biaxial yielding behaviour of highly oriented polypropylene tube

N. E. BEKHET
Department of Mechanical Design, Faculty of Engineering and Technology, El-Matariah, Helwan University, Cairo, Egypt

D. C. BARTON, G. CRAGGS
Department of Mechanical Engineering, Leeds University, Leeds LS2 9JT, UK

Polypropylene tubes with highly oriented molecular structures induced by die-drawing have been tested at various axial/hoop stress ratios to study the first quadrant (tensile–tensile) failure surface with particular regard to the effect of draw ratio. The experimental tests have been conducted on a flexible test rig designed for testing flat sheet and tube under different loading conditions whilst controlling the applied strain rate to within 120–200 s^{-1}. A microcomputer-based system has been developed to control the test and automatically log the data. The experimental results are compared with the predictions of the available anisotropic failure theories. The first-quadrant failure surfaces obtained indicate that the yield behaviour of polypropylene in both isotropic and anisotropic states is hydrostatic-pressure dependent with the degree of pressure dependency increasing with draw ratio. The anisotropic tubes are very weak in the hoop direction compared to the axial direction even when biaxially drawn, and yield by rapid circumferential expansion except when the applied axial stress is very much greater than the hoop stress.

1. Introduction

In recent years there have been numerous studies of the solid-phase deformation of polymers as a method for producing high-stiffness materials in the form of rod, sheet and tube. Solid-state deformation in polymers can be produced by a number of processes such as tensile drawing [1, 2], hydrostatic extrusion [3, 4], ram extrusion [5] and, recently, die-drawing [6–9]. It has been shown that the die-drawing process is preferable because of the relatively high production rates, ease of operation and applicability to nearly all the common thermoplastics [9]. Also die-drawing has the added advantage of offering scope for incorporation into a continuous process (i.e. granules → continuous extrusion of billet → die-drawn product).

As yet, the full potential of drawn polymers cannot be utilized since sufficient data and a generally accepted design procedure have not been established for these highly anisotropic materials. Polypropylene (PP) flat sheet and tube drawn to various draw ratios have previously been tested under uniaxial tensile loading conditions [10, 11]. This study indicated that the longitudinal elastic modulus and yield stress are significantly increased with increasing draw ratio. For high draw ratios, flat sheet has a very much higher elastic modulus and yield stress than the tube material which is usually biaxially drawn to some degree.

A previous study of the tensile and compression plastic deformation of oriented PP sheet [12] showed that oriented crystalline polymers may require different yield criteria for different types of stress state. Earlier studies [13] of polymer rod drawn up to a limited draw ratio showed that the yield behaviour of the oriented polymer may be pressure-dependent. In the present paper, the effect of draw ratio of die-drawn PP tube on the shape and size of the yield surface and on the degree of pressure dependency are considered. In addition, the first-quadrant yield loci of well-known anisotropic yield criteria are compared with the experimental results. These yield criteria are first defined and the two-dimensional failure surfaces that they represent are illustrated for various degrees of strength anisotropy and pressure dependency. The materials and specimen preparation are then briefly described before the test rig and procedure are outlined in some detail. The processing of experimental results is then covered including the fitting of theoretical yield surfaces (simplified to three basic models) to the experimental points. Finally, comparisons are made between the results for different draw ratios, particularly concerning the relative strengths and degree of pressure dependency.

2. Theoretical yield surfaces

The following section discusses the significance of and differences between the various failure theories proposed for anisotropic materials. In this context, failure is defined as the onset of plastic flow (yield) in the material. The well-known anisotropic two-dimensional yield criteria considered in the present work are listed below.

0022–2461

2.1. Maximum stress theory

Failure occurs when

$$\sigma_1 = X \quad \text{or} \quad \sigma_2 = Y \quad \text{or} \quad \tau_{12} = S \quad (1)$$

where $\sigma_1, \sigma_2, \tau_{12}$ are the direct stresses and shear stress in the principal material directions and X, Y, S are the principal direct failure stresses and shear failure stress, respectively.

2.2. Distortional energy theories

Failure occurs according to one of the following distortional energy criteria:

(a) Hill's theory [14]:

$$\left(\frac{\sigma_1}{X}\right)^2 + \left(\frac{\sigma_2}{Y}\right)^2 - \sigma_1\sigma_2\left(\frac{1}{X^2} + \frac{1}{Y^2} - \frac{1}{Z^2}\right) + \left(\frac{\tau_{12}}{S}\right)^2 = 1 \quad (2)$$

where Z is the transverse (out-of-plane) failure stress.

(b) Azzi–Tsai theory [15]:

$$\left(\frac{\sigma_1}{X}\right)^2 + \left(\frac{\sigma_2}{Y}\right)^2 - \frac{\sigma_1\sigma_2}{X^2} + \left(\frac{\tau_{12}}{S}\right)^2 = 1 \quad (3)$$

(c) Norris–McKinnon theory [16]:

$$\left(\frac{\sigma_1}{X}\right)^2 + \left(\frac{\sigma_2}{Y}\right)^2 - \frac{\sigma_1\sigma_2}{XY} + \left(\frac{\tau_{12}}{S}\right)^2 = 1 \quad (4)$$

$$\text{or} \quad \left(\frac{\sigma_1}{X}\right)^2 = 1 \quad \text{or} \quad \left(\frac{\sigma_2}{Y}\right)^2 = 1$$

(d) Fisher theory [17]:

$$\left(\frac{\sigma_1}{X}\right)^2 + \left(\frac{\sigma_2}{Y}\right)^2 - K_2\frac{\sigma_1\sigma_2}{XY} + \left(\frac{\tau_{12}}{S}\right)^2 = 1 \quad (5)$$

where

$$K_2 = \frac{E_1(1+\nu_{21}) + E_2(1+\nu_{12})}{2[E_1E_2(1+\nu_{12})(1+\nu_{21})]^{1/2}}$$

is based on the principal in-plane elastic constants.

(e) Hoffman theory [18]:

(i) Transversely isotropic material theory:

$$\frac{(\sigma_1^2 - \sigma_1\sigma_2)}{X_tX_c} + \frac{\sigma_2^2}{Y_tY_c} + \left(\frac{X_c - X_t}{X_tX_c}\right)\sigma_1 + \left(\frac{Y_c - Y_t}{Y_tY_c}\right)\sigma_2 + \left(\frac{\tau_{12}}{S}\right)^2 = 1 \quad (6a)$$

(ii) Orthotropic material theory:

$$\frac{\sigma_1^2}{X_tX_c} + \frac{\sigma_2^2}{Y_tY_c} - \left(\frac{1}{X_tX_c} + \frac{1}{Y_tY_c} - \frac{1}{Z_tZ_c}\right)\sigma_1\sigma_2 + \left(\frac{X_c - X_t}{X_tX_c}\right)\sigma_1 + \left(\frac{Y_c - Y_t}{Y_tY_c}\right)\sigma_2 + \left(\frac{\tau_{12}}{S}\right)^2 = 1 \quad (6b)$$

where X_t, Y_t, Z_t are direct tensile strengths and X_c, Y_c, Z_c are direct compressive strengths in the 1, 2, 3 directions, respectively.

(f) Caddell *et al.* theory [12]:

$$H(\sigma_1 - \sigma_2)^2 + F(\sigma_2 - \sigma_3)^2 + G(\sigma_3 - \sigma_1)^2 + 2N\tau_{12}^2 + 2L\tau_{23}^2 + 2M\tau_{13}^2 + K_x\sigma_1 + K_y\sigma_2 + K_z\sigma_3 = 1 \quad (7)$$

where

$$H + G = \frac{1}{X_tX_c}, \quad F + H = \frac{1}{Y_tY_c}, \quad G + F = \frac{1}{Z_tZ_c},$$

$$K_x = \frac{X_c - X_t}{X_tX_c}, \quad K_y = \frac{Y_c - Y_t}{Y_tY_c}, \quad K_z = \frac{Z_c - Z_t}{Z_tZ_c}$$

(g) Modified Marin theory [19]:

$$\frac{\sigma_1^2 - K_2\sigma_1\sigma_2}{X_tX_c} + \frac{\sigma_2^2}{Y_tY_c} + \left(\frac{X_c - X_t}{X_tX_c}\right)\sigma_1 + \left(\frac{Y_c - Y_t}{Y_tY_c}\right)\sigma_2 + \left(\frac{\tau_{12}}{S}\right)^2 = 1 \quad (8)$$

where K_2 is defined as for the Fisher theory above.

2.3. Strength tensor theory

These conditions can be written in condensed tensor notation or expanded as shown below.

(a) Gol'denblat–Koponov theory [20]:

$$\frac{X_c - X_t}{2X_tX_c}\sigma_1 + \frac{Y_c - Y_t}{2Y_tY_c}\sigma_2 + \left[\left(\frac{X_c + X_t}{2X_tX_c}\right)^2\sigma_1^2 + \left(\frac{Y_c + Y_t}{2Y_tY_c}\right)^2\sigma_2^2 + 2F_{12}\sigma_1\sigma_2 + \left(\frac{\tau_{12}}{S}\right)^2\right]^{0.5} = 1 \quad (9)$$

where $F_{12} = 0.5/(X_tX_cY_tY_c)^{1/2}$.

(b) Tsai–Wu theory [21]:

$$\frac{X_c - X_t}{X_tX_c}\sigma_1 + \frac{Y_c - Y_t}{Y_tY_c}\sigma_2 + \frac{\sigma_1^2}{X_tX_c} + \frac{\sigma_2^2}{Y_tY_c} + 2F_{12}\sigma_1\sigma_2 + \left(\frac{\tau_{12}}{S}\right)^2 = 1 \quad (10)$$

where F_{12} is as for the Gol'denblat–Koponov theory above.

Different degrees of (yield) strength anisotropy are illustrated in Figs 1–3 in order to indicate the differences between the above failure theories. Fig. 1 shows the failure envelopes for the isotropic case when $X_t = X_c = Y_t = Y_c = Z_t = Z_c$. The distortional energy theories are identical to the tensor theories with $F_{12} = -0.5/X_tY_t$, because the linear terms in σ_1 and σ_2 become zero and the $\sigma_1\sigma_2$ cross-term has a coefficient of 1. All theories lie within the maximum stress theory boundary in the second and fourth quadrants and the Norris and McKinnon theory and the tensor theories are contained within this boundary in all quadrants.

Fig. 2 represents the case where the tensile and compressive strengths are of different magnitude but $X_t = Y_t = Z_t$ and $X_c = Y_c = Z_c$. Hoffman's envelope is identical to that of the modified Marin and tensor

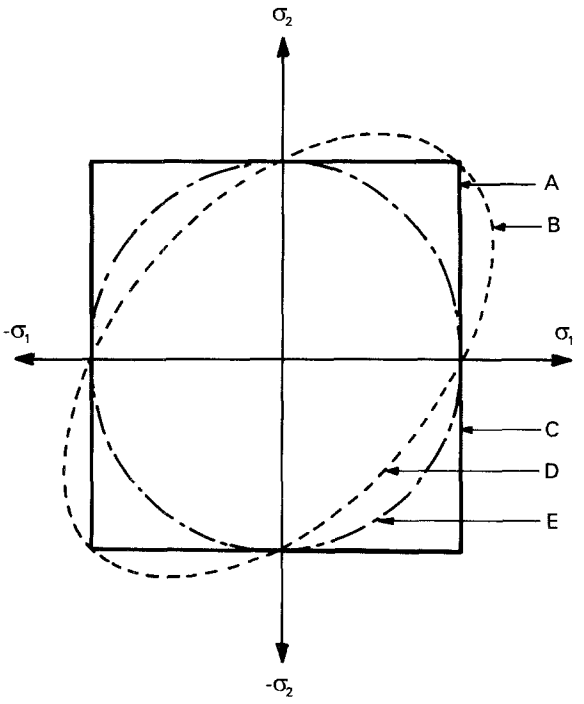

Figure 1 Various yield theories in biaxial stress space for isotropic, pressure-independent material ($X_t = Y_t = X_c = Y_c$): (A, C) maximum stress theory; (A, D) Norris–McKinnon failure theory; (E) modified Marin theory ($K_2 = 0$), tensor theory ($F_{12} = 0$) and Hill's theory; (B) Azzi–Tsai theory, Hoffman theory, modified Marin theory ($K_2 = 1$), tensor theories ($F_{12} = -0.5/X_t X_c$) and Fisher theory ($K_2 = 1$).

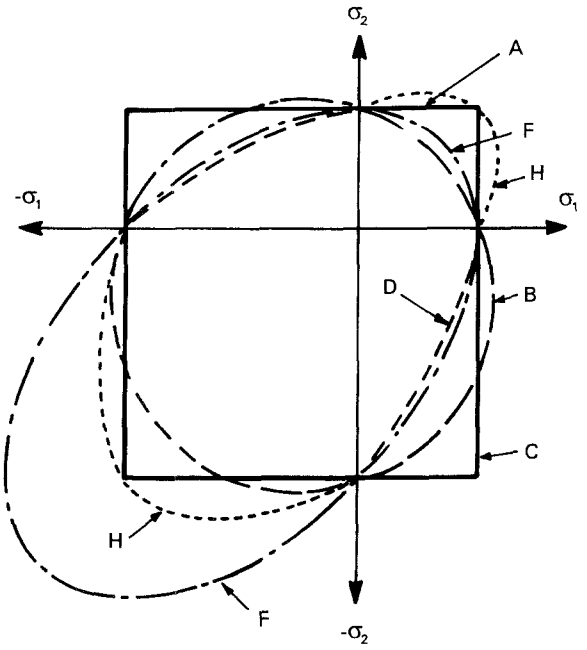

Figure 2 Various yield theories in biaxial stress space for isotropic, pressure-dependent material ($X_t = Y_t = 0.5\,X_c = 0.5\,Y_c$): (A, C) maximum stress theory; (A, D) Norris–McKinnon failure theory; (B) Tsai–Wu theory ($F_{12} = 0$), Gol'denblat–Koponov theory and modified Marin theory ($K_2 = 0$); (F) Hoffman theory, tensor theories ($F_{12} = -0.5/X_t X_c$) and modified Marin theory ($K_2 = 1$); (D, H) Fisher theory ($K_2 = 1$).

theories (with $F_{12} = -0.5/X_t X_c$) because the cross-term coefficients are the same. For Hoffman's theory, $Y_t Y_c$ is assumed equal to $Z_t Z_c$ which eliminates the latter. The failure ellipse for these theories falls within

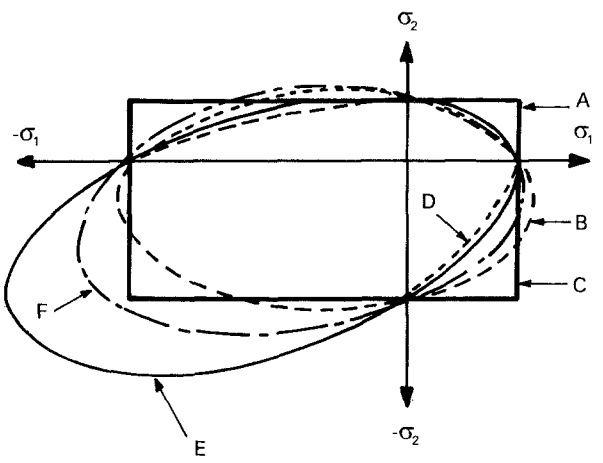

Figure 3 Various yield theories in biaxial stress space for anisotropic, pressure-dependent material ($X_t = 2Y_t = 0.4X_c = 0.8Y_c$): (A, C) maximum stress theory; (A, D) Norris–McKinnon failure theory; (B) Tsai–Wu theory ($F_{12} = 0$), Gol'denblat–Koponov theory and modified Marin theory ($K_2 = 0$); (E) tensor theory ($F_{12} = -1.0/X_t X_c$) and modified Marin theory ($K_2 = 2$); (F) Hoffman theory.

the maximum stress boundary in three quadrants and its origin has moved along the symmetry axis $\sigma_1 = \sigma_2$.

Fig. 3 represents a substantial yield strength anisotropy ($X_t = 2Y_t = 0.4X_c = 0.8Y_c$). In this case, the Hoffman and Tsai–Wu envelopes (with $F_{12} = -1.0/X_t X_c$) are dissimilar since the cross-term coefficient of the latter equation is twice that of Hoffman's, but the differences only become marked in the third quadrant. It can be seen from Fig. 3 that some theories have lost their smooth transition between quadrants, and the origins of the elliptical envelopes have suffered translation although this no longer occurs along the symmetry axis $\sigma_1 = \sigma_2$.

3. Experimental procedure

3.1. Materials and specimen preparation

The material investigated in the present work is highly oriented polypropylene tube (ICI grade GSE 108) produced from tubular billets on a hot die-drawing rig designed and built in the Physics Department of Leeds University. In addition to a high axial drawing ratio, some of the tubes were slightly drawn in the hoop direction by using a mandrel with a diameter larger than the bore of the tubular billet. The degree of material deformation is characterized by the actual axial and hoop drawing ratios R_a and R_h which can be expressed in terms of the initial and final dimensions of the product as follows [8]:

$$R_a = \frac{(D_0^2 - D_i^2)_b}{(D_0^2 - D_i^2)_p} \quad R_h = \frac{(D_0 + D_i)_p}{(D_0 + D_i)_b}$$

where D_0 and D_i are the actual external and internal diameters, respectively, and subscripts b, p refer to the initial billet and final product, respectively. In the present work, billets with $D_0 = 26.0$ mm and $D_i = 18.5$ mm were used throughout. Final product dimensions are shown for each group of specimens in Table I along with the corresponding axial and hoop draw ratios. Group 1 represents undrawn (assumed

TABLE I Summary of results

Group No.	Final product dimensions (mm)		Draw ratios		Uniaxial yield stress (MPa)		Model 1 ($C_1 = C_2 = 1$)	Model 2 ($C_0 = 1$)	
	D_i	D_0	R_a	R_h	X_t	Y_t	C_0	C_1	C_2
1	34.1	32.2	1.0	1.0	10.5	11.0	1.20	0.91	1.65
2	24.0	20.2	2.3	1.0	13.8	11.5	1.40	0.66	0.60
3	30.0	29.0	5.1	1.3	30.0	15.7	1.96	0.58	0.70
4	26.0	25.0	6.8	1.1	41.2	16.2	3.34	0.20	0.40
5	44.5	44.0	7.9	2.0	44.0	17.9	2.23	0.48	0.65
6	36.0	35.4	9.5	1.6	48.8	16.9	3.81	0.14	0.14

isotropic) tube material of dimensions as shown which was tested in the same manner as the drawn product for comparison purposes. In all case, specimens of length 180 mm were cut from the tubular product.

3.2. Test techniques

A flexible test rig specifically designed for both uniaxial and biaxial tests of polymer tube specimens [10] was used in the present experimental work. The loading frame is shown in Fig. 4. The uniaxial longitudinal tensile test was conducted by supplying oil at a controlled rate to an upper hydraulic cylinder (not shown), the axial force from which was transmitted through the tensile bar (with the fixing plate removed) to the mounted specimen. The hoop uniaxial loading test was conducted by using the fixed-end test arrangement shown in Fig. 4 and directing the oil to internally pressurize the tube. In this test, the top end of the tube is free to slide over the end cap which is held rigidly in place so that negligible longitudinal load is applied. In some cases, where the tube was very flexible because it was so thin, two initially loose-fitting Jubilee clips were used to keep the end of the tube in contact with the O-ring seal of the upper end-cap. This minimized oil leakage past the seal whilst allowing the specimen to slide freely over the end-cap.

The tube specimen was biaxially loaded by applying internal pressure and axial tensile load simultaneously from the same hydraulic supply. The axial/hoop stress ratio R in the tube wall therefore depends on the size of the hydraulic loading cylinder and the tube dimensions. Three tensile loading cylinders with inner diameters of 25, 50 and 90 mm were available which provided three values of stress ratio R for each specimen size. Two further values of R were obtained without using the tensile loading cylinder. Firstly, a stress ratio of 0.5 was achieved by internally pressurizing the tube (with clamped ends) while allowing the tensile bar to move freely. Secondly, a stress ratio $R = \nu_{\phi\theta}$, where $\nu_{\phi\theta}$ is the Poisson's ratio in the axial–hoop plane of the tube, could be achieved by completely constraining the tube ends during internal pressurization. This loading configuration is shown in Fig. 4 where two Jubilee clips are used to clamp the top end of the specimen to the end-cap which in turn is rigidly fixed to the middle plate of the test rig.

The rig is computerized so that, using strain gauges mounted on the outside surface of the specimen to monitor the strain, the test could be under maximum principal strain-rate control. All tests were conducted at maximum principal strain rates of 120–200 s^{-1}, room temperature and atmospheric pressure. Hydraulic pressure and hoop and axial strains were monitored throughout each test using a data acquisition system installed on an IBM PC. Where possible, at least four specimens of each group were tested under each condition to allow for scatter in the results.

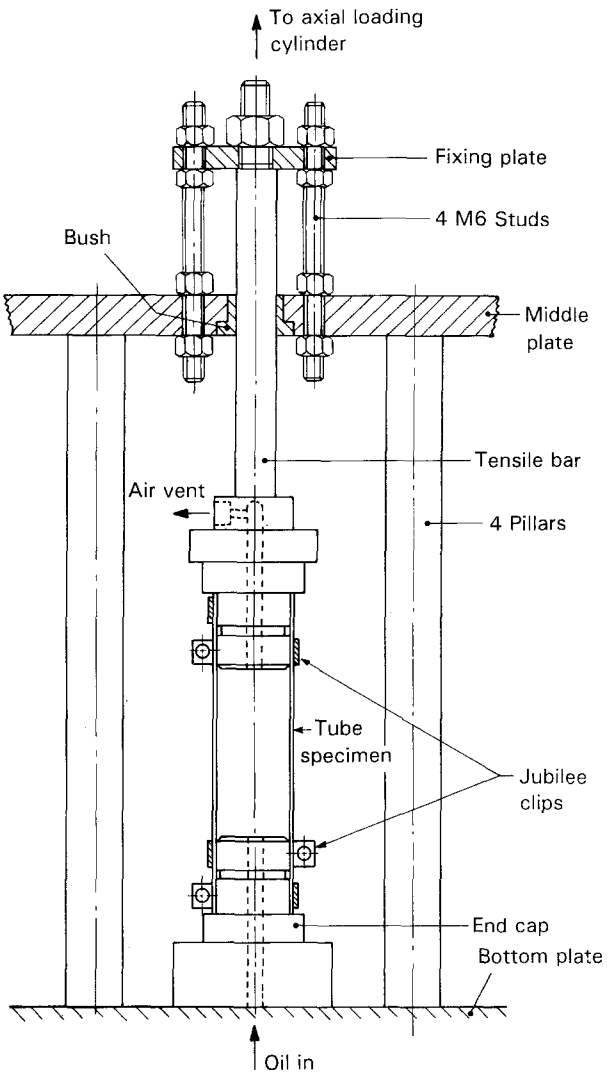

Figure 4 Tube test rig.

4. Results and discussions

4.1. Processing of experimental results

For all test conditions, the axial and hoop stresses in

the tube, σ_ϕ and σ_θ respectively, are proportionally to the hydraulic pressure p:

$$\sigma_\phi = Z_1 p \quad \sigma_\phi = Z_2 p \tag{11}$$

The value of the proportional constants Z_1 and Z_2 depends on the loading conditions. Thus, for uniaxial longitudinal loading

$$Z_1 = A/\pi Dt \quad Z_2 = 0 \tag{12}$$

where A is the cross-sectional area of the hydraulic cylinder and D, t are the tube specimen mean diameter and thickness, respectively. For uniaxial hoop loading

$$Z_1 = 0 \quad Z_2 = D/2t \tag{13}$$

For biaxial loading using the hydraulic cylinder to apply the axial load, we obtain

$$Z_1 = \frac{D}{4t} + \frac{A}{\pi Dt} \quad Z_2 = \frac{D}{2t} \tag{14}$$

For biaxial loading with free end conditions ($R = 0.5$)

$$Z_1 = D/4t \quad Z_2 = D/2t \tag{15}$$

Finally, for fixed ends ($R = \nu_{\phi\theta}$)

$$Z_1 = \nu_{\phi\theta} D/2t \quad Z_2 = D/2t \tag{16}$$

Since σ_ϕ, σ_θ are principal stresses compared with which the corresponding radial stress is considered negligible, the von Mises equivalent stress σ_{eq} for all the above loading conditions is simply

$$\sigma_{eq} = \left\{\frac{1}{2}\left[(\sigma_\phi - \sigma_\theta)^2 + \sigma_\phi^2 + \sigma_\theta^2\right]\right\}^{1/2}$$

$$= p(Z_1^2 + Z_2^2 - Z_1 Z_2)^{1/2} \tag{17}$$

The corresponding equivalent strain ε_{eq} is defined from the measured tube axial and hoop strains ε_ϕ, ε_θ:

$$\varepsilon_{eq} = \left\{\frac{2}{9}\left[\left(\varepsilon_\phi - \varepsilon_\theta\right)^2 + \varepsilon_\phi^2 + \varepsilon_\theta^2\right]\right\}^{1/2} \tag{18}$$

The above relations (with $\nu_{\phi\theta}$ determined from previous uniaxial tests of the same draw ratio tube [22]) were used to plot σ_{eq} versus ε_{eq} for all tests. Best-fit polynomials were then obtained from each set of test data.

Fig. 5 shows the resulting equivalent stress–strain curves under various stress ratios R for specimens of axial draw ratio 6.8. It can be seen that, as R increases, the material appears stiffer and stronger except when $R = \infty$ (uniaxial longitudinal tension). For $R = 0$, 0.5 and 2.2 the material yielded primarily due to hoop loading as evidenced by "ballooning" of the tube and subsequent decrease of the axial strain gauge readings. Thus the stress–strain curve beyond the yield point for $R = 0.5$ in particular is nearly parallel to the hoop uniaxial test response ($R = 0$). Fig. 6 illustrates this phenomenon more clearly since it includes axial, hoop and equivalent stress–strain curves for a biaxial test with $R = 2.5$. The reason for yield occurring primarily due to hoop loading is the low circumferential strength of the tube, since it was highly drawn in the axial direction only. Only when the biaxial stress ratio was raised to 6.5 or more did specimens of this draw

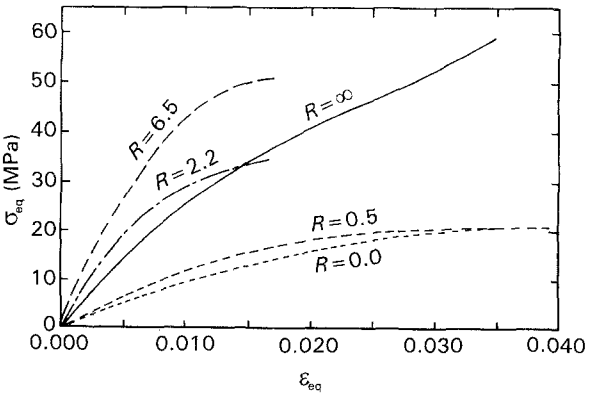

Figure 5 Equivalent stress–strain curves for group 4 drawn tube under various axial/hoop stress ratio R.

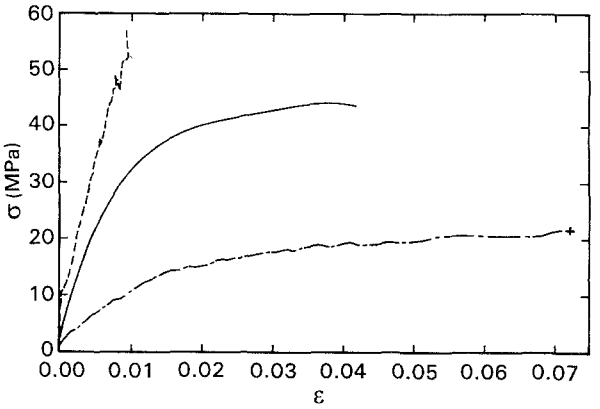

Figure 6 Stress–strain curves for group 5 drawn tube under axial/hoop stress ratio $R = 2.5$. (——) Equivalent stress–strain, (– – –) axial stress–strain, (—·—) hoop stress–strain; (+) failure of strain gauges.

ratio yield primarily due to longitudinal loading as evidenced by rapid axial stretching of the tube.

Hypothetically, the equivalent stress–strain behaviour for isotropic material at all stress ratios should follow the unique uniaxial stress–strain curve. The equivalent stress–strain curves for undrawn PP tube at various stress ratios R are shown in Fig. 7 from which it can be seen that there is relatively little difference between the curves at different stress ratios compared to the drawn tube results shown in Fig. 5. The differences that do exist indicated that the billet material is not truly isotropic.

It is obvious from the typical results presented that, as with most polymers, the PP tube does not exhibit a well-defined yield point for any of the loading conditions considered. Therefore, in order to obtain a consistent and meaningful definition of yield for plotting of the biaxial failure surfaces, the 0.5% proof stress was determined from each equivalent stress–strain curve. This was measured in the usual manner from the intercept of the stress–strain curve with a straight line parallel to the initial elastic part of the curve and passing through 0.5% offset strain. The corresponding "yield" pressure can be obtained from this stress using Equation 17 and finally the corresponding axial and hoop stresses for plotting the biaxial failure surface from Equation 11, using of course the appropriate values of Z_1 and Z_2 for the loading conditions.

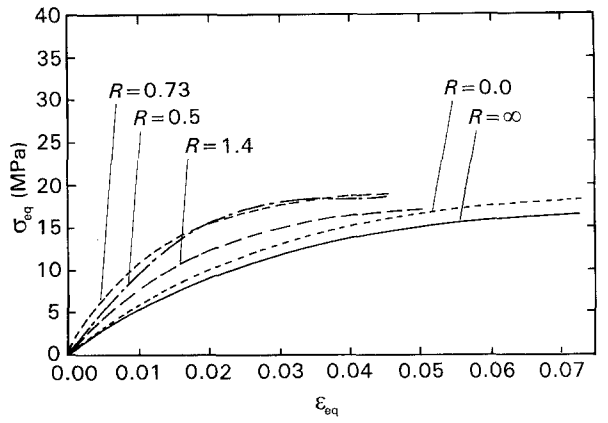

Figure 7 Equivalent stress–strain curves for group 1 undrawn tube under various axial/hoop stress ratios R.

4.2. Determination of yield surfaces

Throughout the following discussion, the uniaxial tensile and compressive yield stresses are denoted as X_t and X_c in the longitudinal direction and Y_t and Y_c in the hoop direction, respectively. Since there was no shear stress applied to the tube specimen when tested under either uniaxial or biaxial loading conditions, the longitudinal and hoop stresses σ_ϕ and σ_θ are considered as principal stresses σ_1 and σ_2, respectively.

The influence of the hydrostatic pressure on the material yielding behaviour has been considered in many yield criteria such as Equations 6–10 by including linear functions of the principal stresses. The coefficients of these linear terms are dependent on the difference between the absolute values of compressive and tensile strengths. Early studies [12, 13, 23, 24] of the yielding behaviour of isotropic and slightly oriented (cold-drawn) polymers indicated that PP and many other polymers are pressure-dependent, i.e. their yield behaviour is affected by the magnitude of the hydrostatic component of stress as shown by differing values of yield stress in tension and compression. Therefore, it was decided to use the pressure-dependent criteria to determine the theoretical yield surface of best fit to the present experimental data. The ratios $C_1 = X_c/X_t$ and $C_2 = Y_c/Y_t$ have been introduced to these criteria as pressure dependency parameters. When $C_1 = C_2 = 1$, the material is considered as pressure-independent; otherwise the material is pressure-dependent. Pressure dependency parameters $C_1 = C_2 = 1.23$ for isotropic PP were obtained by Pae [23]. Caddell *et al.* [13] showed that thin-walled tubes machined from slightly cold-drawn PP rod ($R_a = 1.8$) are pressure-dependent with $C_1 = 0.76$ and $C_2 = 0.64$. On the other hand, pressure dependency parameters $C_1 = 0.16$ and $C_2 = 2.1$ for highly oriented PP sheet ($R_a \simeq 6.5$) were obtained by Shinozaki and Groves [25]. These studies in general indicate that PP in both isotropic and anisotropic states is pressure-dependent, but there is no consensus on values for the pressure dependency parameters.

The yield criterion proposed by Tsai and Wu [21] and the modified Marin theory proposed by Franklin [19] are considered in the present analysis since they can both be simplified to correspond to most of the other theories. These criteria have floating constants K_2 and F_{12} in addition to the pressure dependency parameters as shown in Equations 8 and 10, respectively. The effect of these floating constants on the yield surface has been detailed [19–21]. These two theories can be generalized in a single form as follows:

$$\sigma_1^2 + C_{12}\frac{X_t^2}{Y_t^2}\sigma_2^2 - C_0\sigma_1\sigma_2 + X_t(C_1 - 1)\sigma_1 + \frac{X_t^2}{Y_t}(C_1 - C_{12})\sigma_2 = C_1X_t^2 \quad (19)$$

where $C_{12} = C_1/C_2$ and C_0 is the floating parameter which is identical to K_2 and $2F_{12}$ in Equations 8 and 10, respectively.

Now, for the case of pure biaxial loading with no accompanying shear stress, this general form of the yield criterion can be reduced to many of the other criteria as follows:

1. If isotropy and pressure independency ($X_c = X_t = Y_c = Y_t$) prevail, the strengths in the different reference directions are equal (i.e. $C_1 = C_{12} = 1$) and, assuming $C_0 = 1$, Equation 19 reduces to the von Mises distortional energy criterion.
2. In the case of anisotropic material and pressure independency ($X_c = X_t \neq Y_c = Y_t$, $C_1 = C_{12} = 1$) and assuming $C_0 = 1$, Equation 19 reduces to the Azzi–Tsai theory [15] given in Equation 3.
3. If the material is anisotropic and pressure-dependent and assuming $C_0 = 1$, Equation 15 reduces to the Hoffman [18] and Caddell *et al.* [12] theories given in Equations 6a and 7, respectively.

To predict the yield surface of a material using Equation 19, the tensile and compressive strengths and at least one biaxial yield stress point must be available. The biaxial data are needed to estimate the floating parameter C_0 once C_1 and C_2 are known. The test rig used in the present work was unable to conduct compressive tests, so it was decided to use curves of best fit to the available data in the first quadrant of stress space to estimate these parameters. The statistical analysis system (SAS) software installed on the AMDAHL computer at Leeds University was used to carry out this curve-fitting analysis. Non-linear procedures [26] were used which require the algebraic form of the equation to be made to fit the data to be specified. Three different model criteria based on Equation 19 were used:

(i) model 1 assumes $C_1 = C_{12} = 1$ and allows the SAS to estimate C_0 (pressure-independent material);

(ii) model 2 assumes $C_0 = 1$ and allows the SAS to estimate C_1 and C_{12} (pressure-dependent material); and

(iii) model 3 makes no assumptions and all three constants C_0, C_1 and C_{12} are estimated by the SAS.

Model 3 with three unknown parameters (C_0, C_1 and C_{12}) was found to describe unlikely yield surfaces for most groups, even in the first quadrant where there is much experimental data, so it was not considered further in the present work. A comparison between the

other two models and the various yield criteria is considered in the following discussion.

Basic yield criteria involved in this comparison are the maximum stress theory, the Azzi–Tsai theory and the Norris and McKinnon theory. Since the Hoffman and Caddell theories include pressure-dependent parameters, the results of applying model 2 described above are relevant to these theories. On the other hand, the modified Marin and Tsai–Wu theories are exactly equivalent to model 3. This model has been rejected for the current set of test data as the curve-fitting exercise produced unlikely yield surfaces. However, both modified Marin and Tsai–Wu theories can also be reduced to either model 1 or model 2 by making the assumption of either pressure-independent or pressure-dependent behaviour, respectively.

Comparisons between predicted and experimental yield stress data measured at 0.5% offset strain are given in Figs 8 and 9 for the range of drawn products. The axes of these figures are the hoop and axial stresses which for pure biaxial loading (no torsion) are also the principal stresses. For the predicted yield surfaces, the longitudinal and hoop tensile strengths X_t and Y_t were taken as the mean experimental values at $R = \infty$ and $R = 0$, respectively.

Considering firstly the undrawn tube (Fig. 8a), it can be seen that the model 2 criterion produces the best fit to the experimental data. Model 1 gives optimistic predictions whilst the Azzi–Tsai and Norris and McKinnon theories are somewhat conservative and the maximum stress criterion even more so. Models 1 and 2 also give the best fit to the experimental data

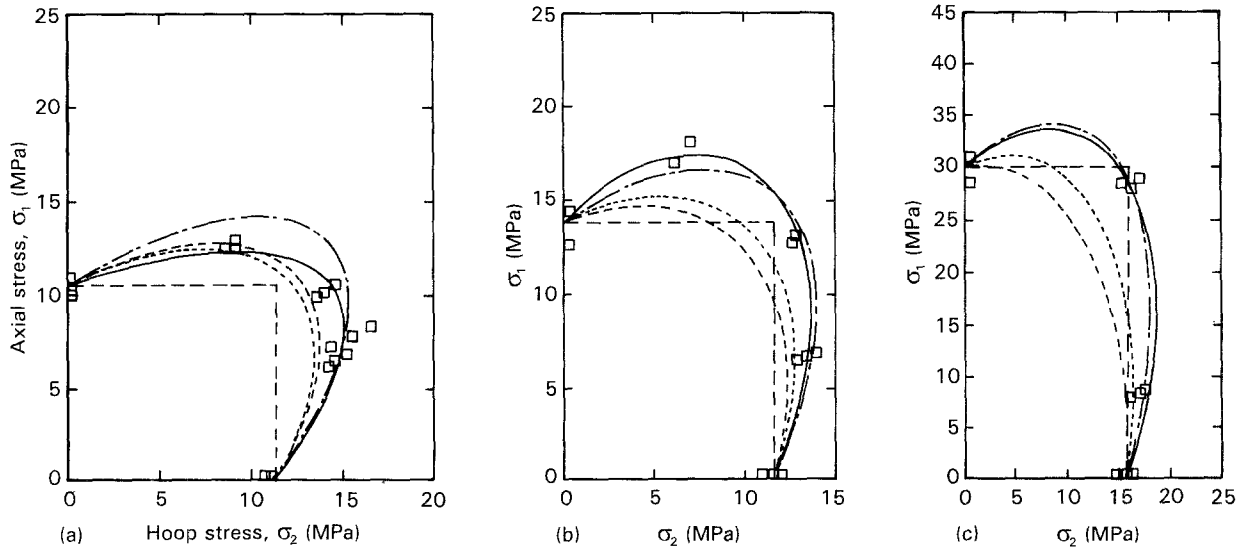

Figure 8 Experimental yield data and best-fit theoretical failure surfaces: (a) Group 1 ($R_a = 1.0$, $R_h = 1.0$); (b) group 2 ($R_a = 2.3$, $R_h = 1.0$); (c) group 3 ($R_a = 5.1$, $R_h = 1.3$). (□) Experimental data, (- - - -) Azzi–Tsai theory, (– – –) Norris–McKinnon failure theory, (— —) maximum stress theory, (— · —) model 1, (——) model 2.

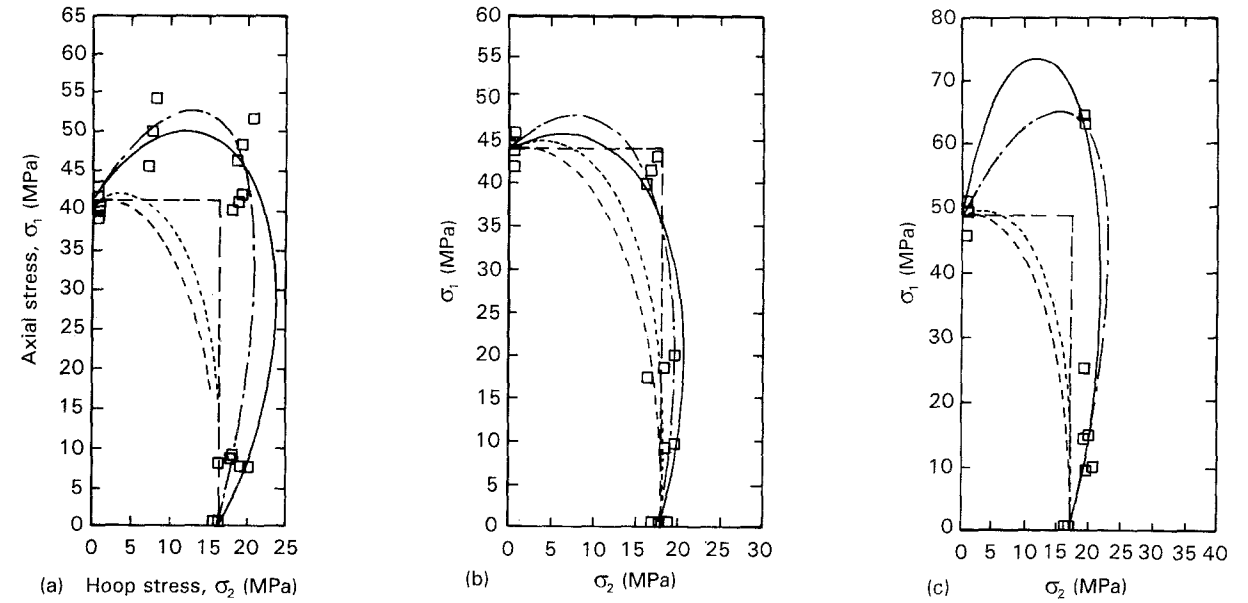

Figure 9 Experimental yield data and best-fit theoretical failure surfaces. (a) Group 4 ($R_a = 6.8$, $R_h = 1.1$); (b) group 5 ($R_a = 7.9$, $R_h = 2.0$); (c) group 6 ($R_a = 9.5$, $R_h = 1.6$). (□) Experimental data, (- - - -) Azzi–Tsai theory, (– – –) Norris–McKinnon failure theory, (— —) maximum stress theory, (— · —) model 1, (——) model 2.

for the remaining groups of drawn tube (Figs 8b, 8c and 9) with, overall, very little advantage to either one. The Azzi–Tsai and Norris and McKinnon criteria are always conservative as is the material stress theory, except perhaps for groups 3 and 5 (Figs 8c and 9).

From the above discussion, it can be concluded that a pressure-dependent anisotropic yield criterion similar to that described by Hoffman [8] and Caddell [12] and designated in the present work as model 2 gives a good fit to the available experimental data. This is in line with the results of Caddell *et al.* [13] for tests on slightly cold-drawn PP rod. However, it should be remembered that data in other quadrants of stress space are required to accurately determine the degree of pressure dependency and that a pressure-independent criterion (model 1) gives almost as good agreement with the first-quadrant experimental results, provided of course that the floating parameter C_0 which is equivalent to K_2 and $2F_{12}$ in the modified Marin and Tsai–Wu theories, respectively, is optimized.

4.3. Further discussion of results

Firstly a word regarding the apparent variability of some groups of experimental results shown in Figs 8 and 9. At most a scatter, defined as the maximum difference between individual data points and the mean result at each stress ratio, of $\pm$ 10% is found in some cases. A possible cause of this scatter is error in the measurement of the specimen diameter, since most specimens tended to be somewhat oval prior to testing. The tube diameter used to calculate the stress was, however, the mean of two diameters measured at each end of the specimen using an internal diameter-measuring micrometer. In addition, the results for groups 5 and 6 initially showed much greater scatter (approx. $\pm$ 20%) in the hoop yield stress value when the mean tube thickness was used in the calculation. After these results were corrected using the local thickness at which the strain gauge was attached, this scatter was reduced to about $\pm$ 10% as for the other groups.

Table I gives the mean uniaxial yield stress data (measured at 0.5% offset strain) for each group of specimens. It can be seen that the longitudinal uniaxial strength increases dramatically as the draw ratio increases. The hoop yield stress is significantly increased for groups 3 to 6 which are slightly drawn in the hoop direction. The curve-fitting results giving C_0 for model 1 and C_1 and C_2 for model 2 are also summarized in Table I. It can be seen that C_0 increases with increasing axial draw ratio R_a (indicating an increased degree of anisotropy) except for group 5, where a decrease is shown compared with group 4. Values of C_1 and C_2 shown in the last two columns of Table I generally decrease with increasing draw ratio. This is an indication that the material is becoming more sensitive to hydrostatic pressure (more pressure-dependent). The exception to the general trend is for group 5 where the C_1 and C_2 values are higher than for group 4 which has a lower axial draw ratio. This implies that biaxially drawn tube is less sensitive to hydrostatic pressure than uniaxially drawn tube of similar axial draw ratio. It therefore seems that hoop drawing has the effect of reducing not only the degree of anisotropy but also the degree of pressure dependency caused by axial drawing.

The model 2 yield surfaces which were found to give the best overall fit to the experimental data are shown superimposed on the same axes for all groups of specimens in Fig. 10. The effect of increasing axial draw ratio is obviously to elongate the near-symmetrical isotropic yield surface towards the axial stress direction. For group 2 specimens which are drawn in the axial direction only, the yield surface at low stress ratios has actually shrunk compared with the isotropic material. The yield surface for group 4 specimens lies mainly outside that for group 5 tubes, which

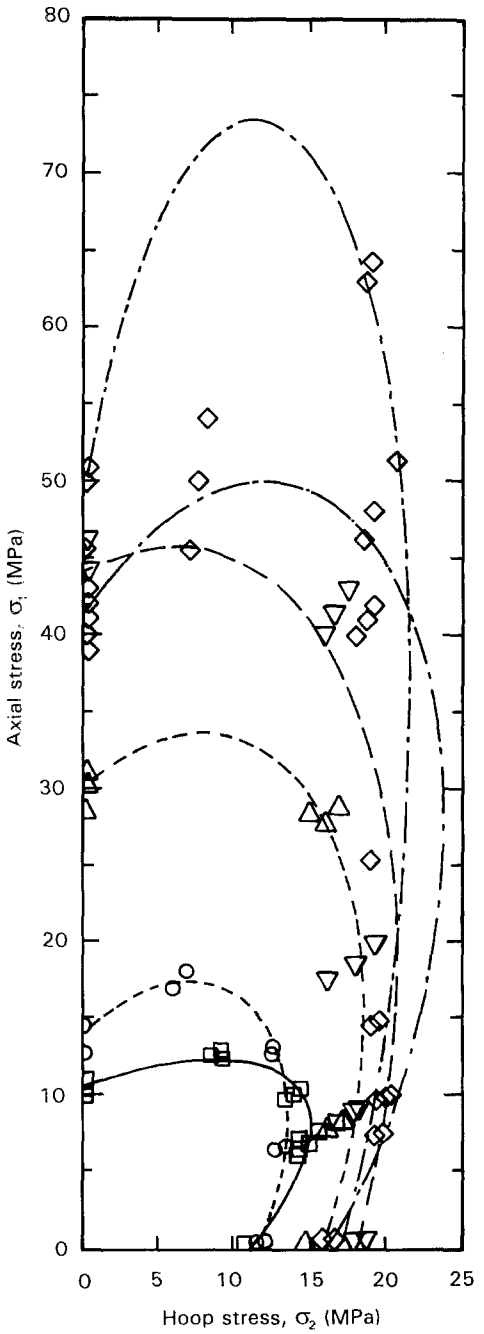

Figure 10 Experimental yield data and best-fit theoretical failure surfaces (model 2) for all groups of specimens: (□, ——) group 1; (○, - - - -) group 2; (△, – – –) group 3; (◇, – – –) group 4; (▽, — —) group 5; (◇, —·—) group 6.

have a somewhat higher axial draw ratio but are much more highly drawn in the hoop direction. This may be because drawing in the hoop direction reduces the degree of molecular orientation arising from simultaneous drawing in the axial direction.

5. Conclusions

1. The uniaxial tensile 0.5% proof stress of drawn polypropylene tube loaded in the longitudinal direction increases dramatically with increasing axial draw ratio. The increase in the corresponding value for uniaxial hoop loading is much more modest because the material is not highly drawn in the hoop direction. Thus the degree of strength anisotropy increases significantly with increasing axial draw ratio.

2. Under biaxial tensile loading, gross yield of the drawn tube produces large displacements in the hoop direction even when the axial stress is much greater than the circumferential value ($R \gg 1$). This further illustrates the relative weakness of the drawn material in the hoop direction.

3. The 0.5% proof stress data when plotted in the first quadrant of biaxial stress space are not well represented by the simpler anisotropic yield criteria such as the maximum stress theory and the Norris and McKinnon and Azzi–Tsai theories. The more complex criteria such as the modified Marin and Tsai–Wu theories give much better agreement provided the floating parameter is optimized in each case. Best overall agreement with the experimental results is given by the pressure-dependent criteria due to Hoffman and Caddell. The optimized pressure dependency constants in these latter indicate a greater effect of the hydrostatic pressure on yield behaviour as the axial draw ratio of the PP tubes is increased.

4. Results such as those presented in this paper should enable highly drawn polymers to be specified with more confidence and less conservatism for situations where the loading is predominantly biaxial tension, as in many pressurized pipe and vessel applications.

References

1. G. COPACCIO, T. A. CROMPTONS and I. M. WARD, *J. Polym. Sci., Polym. Phys. Ed* **18** (1980) 301.
2. A. J. WILLS, G. COPACCIO and I. M. WARD, *ibid.* **18** (1980) 493.
3. K. NAKAMURA, K. IMADA and M. TAKAYANAGI, *Int. J. Polym. Mater.* **18** (1972) 71.
4. P. S. HOPE, A. G. GIBSON, B. PARSONS and I. M. WARD, *Polym. Eng. Sci.* **18** (1980) 540.
5. S. MARUYAMA, K. IMADA and M. TAKAYANAGI, *Int. J. Polym. Mater.* **2** (1973) 125.
6. A. TARAIYA, A. RICHARDSON and I. M. WARD, *J. Appl. Polym. Sci.* **33** (1987) 2559.
7. A. RICHARDSON, B. PARSONS and I. M. WARD, *Plast. Rubb. Process. Appl.* **6** (1986) 347.
8. A. TARAIYA, Ph.D. thesis, Leeds University (1989).
9. B. SELWOOD, I. M. WARD and B. PARSONS, *Plast. Rubb. Process. Appl.* **8** (1987) 49.
10. N. E. BEKHET, Ph.D. thesis, Leeds University (1989).
11. N. E. BEKHET, D. C. BARTON and G. CRAGGS, *Poly. Testg* **12** (1993) 401.
12. R. M. CADDELL, R. S. RAGHAVA and A. G. ATKINS, *J. Mater. Sci.* **8** (1973) 1641.
13. R. M. CADDELL and A. R. WOODLIFF, *ibid.* **12** (1977) 2028.
14. R. HILL, *Proc. Roy. Soc. A* **193** (1948) 281.
15. V. D. AZZI and S. W. TSAI, *Exp. Mechan.* (1965) 283.
16. C. B. NORRIS and P. F. MCKINNON, "Compression, tension and shear plywood panels of sizes that do not buckle with tests made at various angles to the face grain", Report No. 1328 (Forest Products Laboratory, 1946).
17. L. FISHER, *J. Eng. Indust.* (1967) 399.
18. O. HOFFMAN, *J. Compos. Mater.* **1** (1967) 200.
19. H. G. FRANKLIN, *Fibre Sci. Tech.* **1**(2) (1968) 137.
20. I. I. GOL'DENBLAT and V. A. KOPNOV, *Mekhanika Polimerov* **1**(2) (1965) 70.
21. S. W. TSAI and E. M. WU, *J. Compos. Mater.* **4** (1970) 58.
22. N. E. BEKHET, D. C. BARTON and G. CRAGGS, *Process. Adv. Mater.* in press.
23. K. D. PAE, *J. Mater. Sci.* **12** (1977) 1209.
24. R. M. CADDEL and J. W. KIM, *Int. J. Mech. Sci.* **23** (1981) 99.
25. D. SHINOZAKI and G. W. GROVES, *J. Mater. Sci.* **8** (1973) 71.
26. J. T. HELWING, "Statistical Analysis System (SAS), SAS Introductory Guide", (SAS Institute, Carrboro, North Carolina, 1978).

Received 1 March
and accepted 28 April 1994